IEEE Access
Multidisciplinary | Rapid Review | Open Access Journal

Received April 8, 2021, accepted May 4, 2021, date of publication May 10, 2021, date of current version May 18, 2021.

Digital Object Identifier 10.1109/ACCESS.2021.3078644

Non-Negative Matrix Factorization of Simulated High Density Surface Electromyograms Reflects Both Muscle Excitation and Muscle Shortening

MARTIN ŠAVC, (Member, IEEE), AND ALEŠ HOLOBAR, (Member, IEEE)
Faculty of Electrical Engineering and Computer Science, University of Maribor, 2000 Maribor, Slovenia

Corresponding author: Martin Šavc (martin.savc@um.si)

This work was supported by the Slovenian Research Agency under Project J2-1731, Project L7-9421, and Project J2-7357 and Program funding P2-0041.

ABSTRACT We analyzed muscle excitation estimation systematically by Non-negative matrix factorization (NMF) from surface electromyograms (EMG) during dynamic contractions of biceps brachii (BB) muscles. We used motor unit action potentials (MUAPs) estimated experimentally from surface EMGs during slow dynamic contractions of BB muscles in healthy young males, and convolved them by simulated motor unit firing patterns. Different uncorrelated muscle excitation and muscle shortening profiles were combined when generating the EMG signals from left and right BBs (64 channels per muscle). EMG signals were rectified, low-passed filtered and decomposed by NMF into 2, 3, 4 or 6 components. The identified NMF components demonstrated good separation of left and right BB activity, but relatively large sensitivity of NMF components to muscle shortening, especially at high levels of muscle excitation. When averaged across different numbers of identified NMF components at excitation levels ranging from 40 to 80%, the average correlation coefficient between the NMF components and muscle shortening profiles was 0.45 ± 0.15. At excitation levels between 0 and 40 % these correlations decreased to 0.15 ± 0.09. Therefore, NMF components reflect both muscle excitation and muscle shortening profiles.

INDEX TERMS Changes of motor unit action potentials, muscle excitation, muscle shortening, non-negative matrix factorization, surface electromyograms, dynamic contractions.

I. INTRODUCTION

In the last two decades, estimation of electrical activity of skeletal muscles from noninvasively acquired surface electromyograms (EMGs) has received considerable attention [1]–[6]. Among other things, it has been used to study muscle synergies [3]–[9], improve the rehabilitation procedures [10], [11], control bionic limbs [12], prosthetic and robotic devices [13], [14] and drive the advanced biomechanical models of human movement [15]. In these applications, the muscle activity is frequently estimated by decomposing the EMG signals into movement primitives or components that are contributed by different skeletal muscles and/or their compartments.

Indeed, a surface EMG is a compound signal, comprising filtered contributions of individual muscle fibers. From a functional viewpoint, the fibers are organized into motor units that vary greatly in their sizes [16]. Each motor unit comprises from a few tens to a few hundreds of muscle fibers and an alpha motor neuron innervating those fibers. In a healthy motor unit, each electrical pulse in a neuron triggers electrical responses, so-called action potentials, in innervated muscle fibers. The action potential propagates via muscle fiber, causing the fiber to contract [16]. All the fibers belonging to the same motor unit contract synchronously, and their simultaneous action potentials can be summed up conceptually into a so-called motor unit action potential (MUAP). The latter is strong enough to support its detection on the surface of the skin above the investigated muscle [1].

There are from several tens to several hundreds of motor units in each skeletal muscle, and the central nervous system (CNS) modulates the muscle force by controlling the number of activated motor units and the number of triggered MUAPs per second, so-called motor unit firing rates [16]. Both factors are referred to jointly as muscle excitation, whereat excitation of 0% implies no active motor unit, and excitation of 100% implies all the motor units firing at their maximum rates. Muscle excitation changes with exercise,

The associate editor coordinating the review of this manuscript and approving it for publication was Zhanpeng Jin.

rehabilitation, fatigue, aging and various pathologies, providing a valuable insight in the functioning of a human motor system [16].

However, a surface EMG may detect the contributions of several skeletal muscles, so-called muscle crosstalk, imposing the need to separate these contributions [17]. Moreover, MUAP shapes depend on the anatomy of a skeletal muscle, on the distance of the motor unit fibers from the uptake electrodes, and on the EMG acquisition parameters. Therefore, MUAPs weight the contributions of different motor units with different pounders, hindering the accurate estimation of muscle excitation from a raw surface EMG.

Different decomposition techniques have been proposed to address this problem [2], [18]–[22], [6], [23], [24]. Some of them aim to identify the contributions of individual motor units [2], [6], [23], [24], but exhibit relatively high computational complexity and motor unit selectivity, identifying the contributions of a limited number of activated motor units. Other decomposition techniques, such as non-negative matrix factorization (NMF) [25], [26], separate the contributions of different muscles, but do not aim to identify the activity of individual motor units.

Up to now, NMF has been used in many peer reviewed studies of the human motor system [3], [4], [7]–[9], [25], providing very important neurophysiological insights. To the best of our knowledge, its sensitivity to MUAP shapes and their changes during dynamic or significantly fatiguing muscle contractions has never been studied systematically. Indeed, in dynamic contractions, the geometry of the muscle changes, causing the changes of MUAPs as detected on the surface of the skin. As shown in [27] and herein, these changes can be substantial. In this study, we analyzed the sensitivity of NMF to MUAP changes of a muscle in different muscle shortening and muscle excitation scenarios.

II. DYNAMIC SURFACE EMG SIMULATION

The EMG signals in this study were synthesized using a collection of MUAPs extracted at different stages of biceps brachii (BB) muscle shortening, a model of MU firing rates [28], and carefully selected excitation and muscle shortening profiles.

A. MUAPs

We used the collection of MUAPs from [27], where the experimental setup and signal processing are described in detail. In short, the MUAPs were extracted from monopolar high-density EMG signals of the right (dominant) BB in five young males (ages of 34.4 $\pm$ 5.4 years, height of 177 $\pm$ 5.1 m and weight of 77.2 $\pm$ 5.5 kg). The subjects performed 80 s long slow isokinetic contractions from a fully extended to a fully flexed elbow. The EMG signals were measured using an array of 13 $\times$ 5 electrodes at a sampling rate of 2048 Hz and 12-bit resolution (EMG-USB2 amplifier, OT Bioelettronica, Torino, Italy).

By using the Convolution Kernel Compensation (CKC) decomposition technique [1], [2] we identified 250 MU firing patterns. These were used to extract 40 ms long MUAPs at 36 different stages of muscle shortening, from fully extended (0% shortening) to a fully flexed elbow (100% shortening). The examples of estimated MUAP shapes are depicted in Fig. 1.

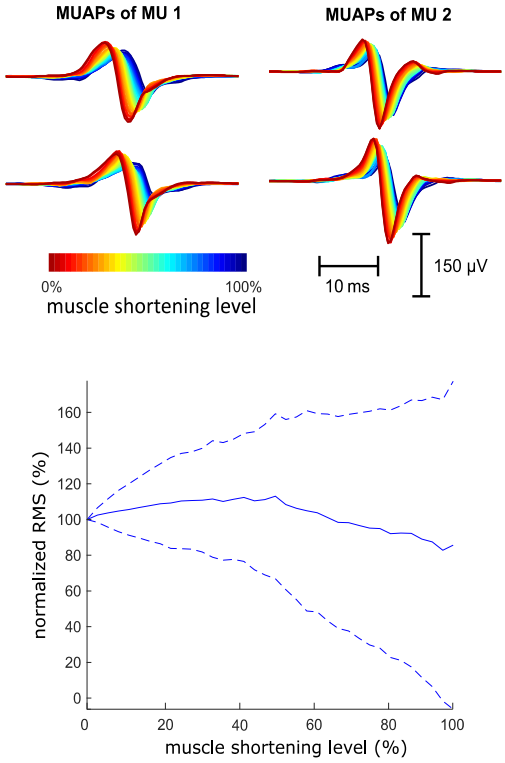

FIGURE 1. Experimentally determined MUAPs, estimated at 36 different levels of Biceps Brachii shortening (upper panel) and the root mean square (RMS) value of MUAPs at different levels of muscle shortening normalized by the RMS value of MUAPs at the fully extended muscle (lower panel). The different colors in the upper panel depict MUAP shapes at different levels of muscle shortening. For clarity reasons, MUAPs of only two MUs in only two neighboring EMG channels are depicted. In the lower panel, the reported values at each shortening level are averaged across 250 MUs identified from five healthy subjects. The solid line depicts the mean value, whereas the dotted lines depict the standard deviations. Note the high diversity of changes with muscle shortening. For some MUs RMS value of MUAPs increased with muscle shortening, whereas for the others it decreased.

B. SIMULATED MUSCLE EXCITATIONS AND MU FIRING PATTERNS IN THE ABSENCE OF MUSCLE CROSSTALK

To test the sensitivity of the NMF components to geometric changes in the investigated muscle, we simulated two BB muscles independently, controlling the activity of the left and right elbow joints. This experimental setup guaranteed the absence of muscle crosstalk in the simulated EMG signals. The simulated BB contractions were 60 s long and followed cosine functions whereat frequencies of the excitation (8/60 Hz for the left and 9/60 Hz for the right BB) and shortening (3/60 Hz for the left and 4/60 Hz for the right BB) were selected carefully, to minimize their correlation and, thus, facilitate the analysis of the NMF components.

Different excitation levels were simulated, defining the minimum and maximum (and, thus, the range) of

excitation profiles. The following ten ranges of excitation were simulated (minimum-maximum): 0-20%, 0-40%, 0-60%, 20-40%, 20-60%, 20-80%, 40-60%, 40-80%, 40-100%. The generated excitation profiles for the left and the right BB muscle are depicted in the top panel of Fig. 2.

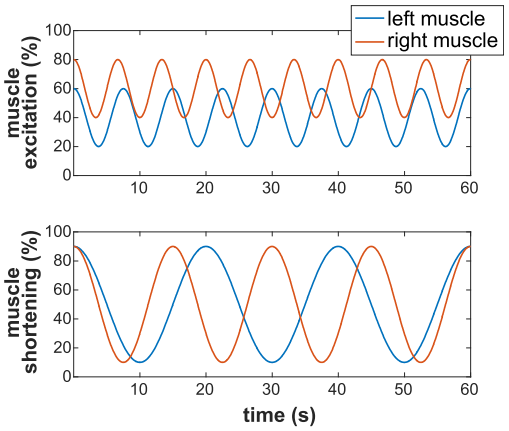

FIGURE 2. Examples of simulated muscle excitation and shortening profiles. The top panel depicts two examples of excitation profiles, one for the left and one for the right BB. The bottom panel depicts the two shortening profiles, spanning from 10% to 90% of muscle shortening. Due to the carefully selected profiles' frequencies, these profiles were not correlated (all pairwise correlation coefficients are equal to zero).

For each simulated muscle excitation profile, MU firings were generated using the model proposed in [28]. MU recruitment followed an exponential distribution, with many low-threshold MUs and fewer high-threshold MUs [29]. In each generated muscle 105 MUs were active in the detection volume of surface electrodes at 100% muscle excitation. MUs started firing at 8 Hz, increasing their firing rates linearly for 0.3 Hz per % of muscle excitation, up to a 35 Hz. The MU interspike interval variability followed a Gaussian distribution with the coefficient of variation set to 20 %.

For each of the excitation profiles, MUAPs of the experimentally identified MUs were assigned randomly to the generated firing patterns. This was done independently for the left and right muscle. The generated MU firing patterns were then convolved with MUAPs, whereat for each firing one of the 36 discrete dynamic MUAP shapes (Fig. 1) was selected, based on the current muscle shortening level. Two uncorrelated muscle shortening profiles were used, one for the left and the other for the right BB. The left and right profiles followed a 3/60 Hz and 4/60 Hz cosine. The ranges of both muscle shortening profiles were fixed to the interval of (minimum-maximum) 10-90% of muscle shortening (Fig. 2, bottom panel).

Two EMG simulation runs were conducted for each possible pair of left and right BB excitation profiles. Thus, within these 162 simulated contractions, each individual excitation profile for one muscle was repeated 18 times, 2 times for each of the 9 excitation profiles of the other muscle.

C. SIMULATED MUSCLE EXCITATIONS IN THE PRESENCE OF MUSCLE CROSSTALK

To analyze the effect of muscle crosstalk on our analysis we simulated a single BB muscle, but divided its MUAPs into short (medial) and long (lateral) heads. The division was based on the position of the channels with maximum peak to peak MUAP amplitude at different shortenings. If most of these channels were positioned in the lateral three electrode columns they were added to the lateral group. Otherwise they were added to the medial group. This division resulted in 40% of MUAPs in the medial, and 60% in the lateral group. Each group was combined with separate excitation and shortening profiles, leading to two distinct groups of muscle activations and shortenings for the lateral and medial head of the muscle. Although not physiologically justified, this division supported a clear discrimination of excitation profiles, and, therefore, quantification of the crosstalk. The profiles of excitation and shortening were the same as above (8/60 Hz for the medial and 9/60 Hz for the lateral head excitation, and 3/60 Hz for the medial and 4/60 Hz for the lateral head shortening profile). However, only the following ranges of excitation were simulated (minimum-maximum): 0-40 %, 20-60 %, 40-80 %. Compared to previously generated signals these had significant levels of muscle crosstalk between the medial and lateral MUAP groups.

III. EMG DECOMPOSITION

A. NMF

The NMF decomposition followed the method proposed in [25]. First, the EMG signals were rectified, and filtered to estimate their amplitude envelopes:

$$z_m(n) = 1/(2\Delta n + 1) \sum_{n_i=n-\Delta n}^{n+\Delta n} y_m^2(n_i), \tag{1}$$

where $y_m(n)$ stands for the n-th sample of the m-th EMG channel, $z_m(n)$ is its energy envelope and $2\Delta n$ is the filter length in samples. The filter length of 200 ms was used.

The resulting envelopes were packed in a matrix $\mathbf{Z}(n) = [z_1(n), z_2(n) \ldots z_M(n)]$, and decomposed by the NMF algorithm [26] into a mixing matrix $\mathbf{W}$ and component matrix $\mathbf{F}$:

$$\boldsymbol{Z}^{(M\times N)} = \boldsymbol{W}^{(M\times J)}\boldsymbol{F}^{(J\times N)}, \tag{2}$$

where J is the chosen number of NMF components, M is the number of EMG channels and N is the number of samples.

In this study, we were interested in estimating up to four different dynamics of EMG signals, two due to muscle shortening and two due to muscle excitation of the left and right BBs. Additional degrees of freedom were allowed, to compensate for potential inaccuracies in the NMF data model, caused primarily by MUAP changes due to muscle shortening. For this reason, we tested several numbers of NMF components, namely, J = 2, 3, 4 and 6.

B. EVALUATION OF DECOMPOSITION RESULTS

To invert the squaring of EMG signals in (1), the components **F** were square rooted and filtered using a 1 s long Hann window. Each filtered component **F** was compared to the muscle excitation and shortening profiles by calculating their Pearson correlation coefficients.

For each EMG simulation run, two NMF components were selected, with the largest energy accounted for in the left and right BB. The correlations of these components with simulated excitation and shortening profiles were examined further.

To confirm the statistically significant differences in the observed correlation coefficients across different excitation profiles, the correlations were first tested for normality by transforming them using the Fisher transformation and performing the Shapiro-Wilk test. The test indicated that some of the correlations were decisively not normal ($p < 0.01$). Further analysis was therefore done by the Kruskal-Wallis rank sum test, and the Wilcoxon rank sum test for pairwise comparison with Bonferroni correction for multiple comparisons. To confirm the differences between the different number of NMF components J in the decomposition, the correlations were compared using the Friedman rank sum test, and Nemenyi test for pairwise comparison. The results were considered statistically significant when $p < 0.05$.

IV. RESULTS

A. SIMULATED MUSCLE EXCITATIONS IN THE ABSENCE OF MUSCLE CROSSTALK

The square rooted and filtered components are depicted in Fig. 3, along with the corresponding mixing vector **w**, denoting the row of the **W** matrix in (2). The elements of mixing vectors **w** are organized in topological order of the surface EMG electrodes, and reflect the energy that the component contributes to each EMG channel. NMF clearly separated the contributions of the left and right BB muscles.

Figs. 4 and 5 depict the correlation coefficients between the identified NMF components for $J = 2$ and $J = 6$, respectively. Each axis shows values from the $[-1, 1]$ interval. In the first row we compare the correlations of the identified NMF components with the excitation of the left (x-axis) and the right muscles (y-axis). These results demonstrate relatively small crosstalk from different muscles in different NMF components, confirming that excitations of both muscles were well separated by NMF. In the second and third row of Figs. 4 and 5 we depict the correlation of the identified NMF components with the excitation profile (x-axis) and shortening profile in the same muscle. We see two clearly separated groups of NMF components. The group in the center of the plots has low correlation with both excitation and shortening profiles, demonstrating again relatively small muscular crosstalk in the NMF components. This was expected, as two spatially well separated muscles were studied. Conversely, the second group of NMF components demonstrates significant correlation with both excitation and shortening profile of the same muscle, indicating the impact of the muscle shortening on the muscle excitation estimation by NMF. If the NMF components were independent from the MUAP shapes, their correlation with the shortening profile would be equal to zero. This is clearly not the case, especially at higher excitation levels (the right columns of Figs. 4 and 5).

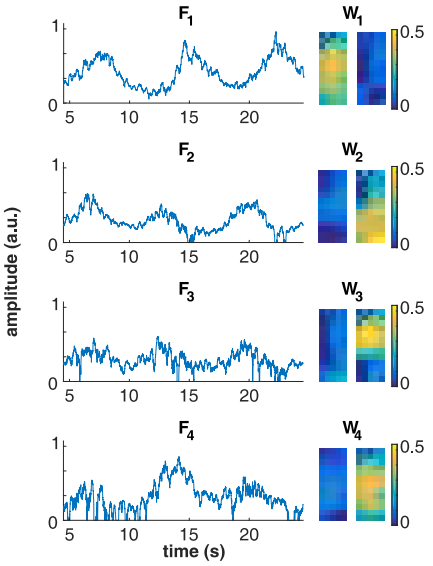

FIGURE 3. Results of NMF decomposition of the EMG signals, generated using the excitation and shortening profiles from Fig. 2. The J = 4 NMF components F1, F2, F3 and F4 are depicted on the left side. The corresponding mixing coefficients, organized in topological order of the two surface EMG electrode arrays, one for the left and one for the right BB, are depicted on the right side. In the depicted case, the NMF identified one component from the left and three components from the right BB muscle.

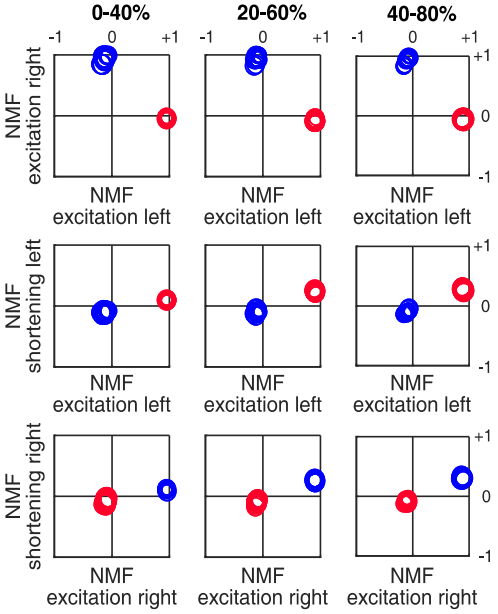

FIGURE 4. Correlation coefficients of the NMF components (J = 2) with shortening and excitation profiles for excitation ranges 0-40%, 20-60% and 40-80% in different columns. Each circle represents a single NMF component, its size representing the energy accounted for in the preprocessed EMG signal. The components that contributed mostly to the right and the left muscle are depicted by blue and red circles, respectively.

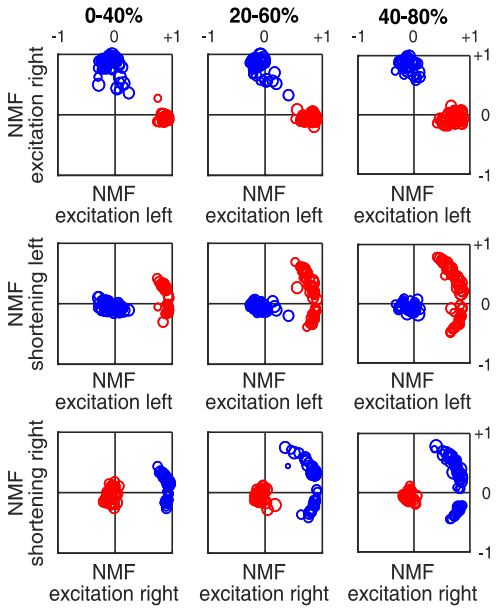

FIGURE 5. Correlation coefficients of NMF components (J = 6) with shortening and excitation profiles for the excitation ranges 0-40%, 20-60% and 40-80% in different columns. Each circle represents a single NMF component, its relative size reflecting the energy accounted for in the preprocessed EMG signal. The components that contributed mostly to the right and the left muscle are depicted by blue and red circles, respectively.

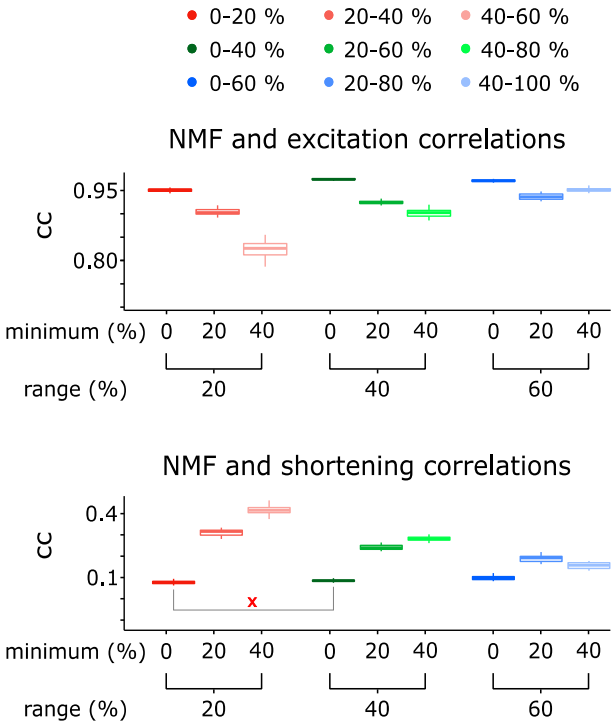

FIGURE 6. Statistical comparison of correlation coefficients (cc) between the NMF components with the largest energy accounted for in the EMG of the right BB muscle, and the muscle excitation (top row) and shortening profiles (bottom row). The number of identified NMF components was set to J = 2. The box plots denote the quartiles, whereas the whiskers denote the range. The plots were grouped by the range of excitation (either 20%, 40% or 60%) and, within each group, sorted by the minimum of excitation (either 0%, 20% or 40%). Pairwise comparisons revealed statistically significant differences ($p < 0.05$) in all the depicted cases, except for the pair marked by a red x.

In the sequel, we focus on the results of the right BB muscle (without simulated muscle crosstalk). Similar results were also observed for the left BB muscle (results not shown). The statistical analyses depicted in Figs. 6 and 7 illuminate the relation between the excitation level and the sensitivity of NMF to the BB shortening. In both studied factors, the minimum of the excitation level and its range (that is, the difference between the maximum and the minimum), had a significant impact. In most cases, an increase in excitation level led to an increase in sensitivity of NMF to muscle shortening (this is best observed within each range group of Figs. 6 and 7). An exception to this was an increase in excitation level from 20% to 40% for the 60% range in the case of J = 2 NMF components.

On the other hand, an increase in excitation range led to a decrease of sensitivity to muscle shortening (this can be observed across the range groups of Figs. 6 and 7). An exception occurred at the excitation level of 0 %, again for NMF with J = 2 components (Fig. 6). Here, an increase of excitation range led to small, but statistically significant increases in sensitivity to muscle shortening. Increasing the number of NMF components to J = 6 led to similar trends in increases of sensitivity to muscle shortening, as in the case of J = 2 components (Fig. 7).

The average correlation coefficients between the NMF components and excitation and shortening profiles for all the simulated contractions and all the NMF decompositions are provided in Tables 1 and 2. In Table 1, the Friedman rank sum test and Nemenyi test for pairwise comparison showed that there were significant differences between column J = 2 and columns J = 3, J = 4 and J = 6, and between columns J = 3 and J = 6. In Table 2, there were significant differences between column J = 2 and columns J = 3, J = 4 and J = 6. In all the cases the p-values were several magnitudes lower than 0.05.

TABLE 1. Correlation coefficients (mean ± SD) between the NMF components with the largest energy accounted for in the right BB, and different excitation profiles at different numbers of NMF components J.

Excitation	J=2	J=3	J=4	J=6
0-20 %	0.95±0.004	0.92±0.073	0.94±0.026	0.88±0.056
0-40 %	0.97±0.002	0.93±0.079	0.93±0.062	0.90±0.053
0-60 %	0.97±0.002	0.89±0.088	0.88±0.108	0.90±0.084
20-40 %	0.90±0.007	0.78±0.154	0.74±0.157	0.71±0.130
20-60 %	0.92±0.004	0.81±0.131	0.80±0.123	0.77±0.142
20-80 %	0.94±0.007	0.81±0.086	0.81±0.091	0.85±0.070
40-60 %	0.82±0.018	0.69±0.128	0.65±0.114	0.57±0.136
40-80 %	0.90±0.009	0.72±0.114	0.74±0.091	0.71±0.112
40-100 %	0.95±0.005	0.86±0.046	0.88±0.056	0.85±0.081

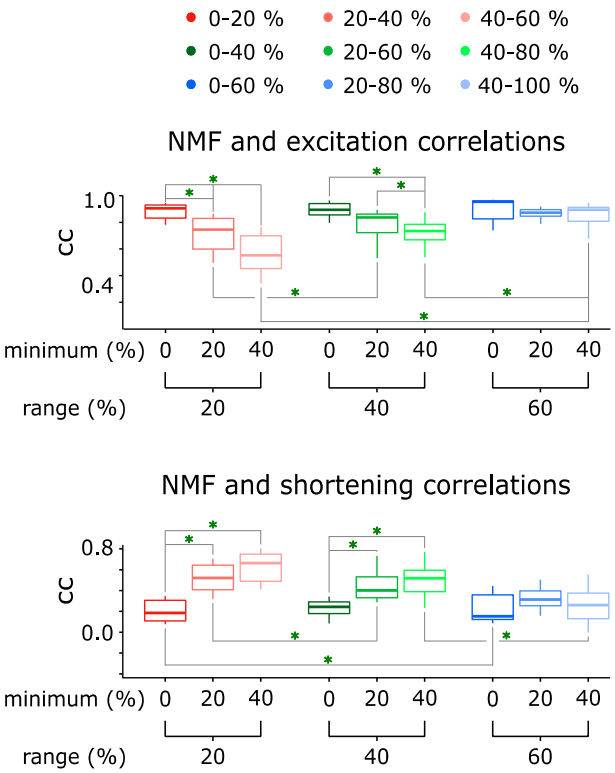

FIGURE 7. Correlation coefficients (cc) between the NMF component with the largest energy accounted for in the EMG and the muscle excitation (top row) and shortening profiles (bottom row). The number of identified NMF components was set to J = 6. The box plots denote the quartiles, whereas the whiskers denote the range. The plots were grouped by the range of excitation (either 20%, 40% or 60%) and, within each group, sorted by the minimum of excitation (either 0%, 20% or 40%). Pairwise statistically significant differences ($p < 0.05$) are marked by *.

TABLE 2. Correlation coefficients (mean ± SD) between the NMF componens with the largest energy accounted for in the right BB, and muscle shortening profile for the different excitation profiles and different numbers of NMF components J.

Excitation	J=2	J=3	J=4	J=6
0-20 %	0.08±0.010	0.10±0.071	0.09±0.055	0.19±0.101
0-40 %	0.08±0.009	0.13±0.083	0.15±0.099	0.22±0.082
0-60 %	0.10±0.011	0.20±0.113	0.22±0.136	0.21±0.133
20-40 %	0.31±0.017	0.43±0.142	0.46±0.149	0.52±0.130
20-60 %	0.24±0.015	0.37±0.144	0.37±0.149	0.43±0.140
20-80 %	0.19±0.021	0.38±0.117	0.39±0.139	0.32±0.099
40-60 %	0.41±0.026	0.54±0.118	0.60±0.112	0.62±0.135
40-80 %	0.28±0.014	0.53±0.133	0.48±0.128	0.49±0.142
40-100 %	0.16±0.015	0.37±0.075	0.26±0.125	0.26±0.166

B. SIMULATED MUSCLE EXCITATIONS IN THE PRESENCE OF MUSCLE CROSSTALK

Fig. 8 depicts the correlation coefficients between identified NMF components for J = 6, using the signals of a single simulated muscle divided into a medial and lateral MUAP group to analyze the effects of the crosstalk. The individual NMF components are not as clearly separated into two groups as in the case of Fig. 5. Although some individual components

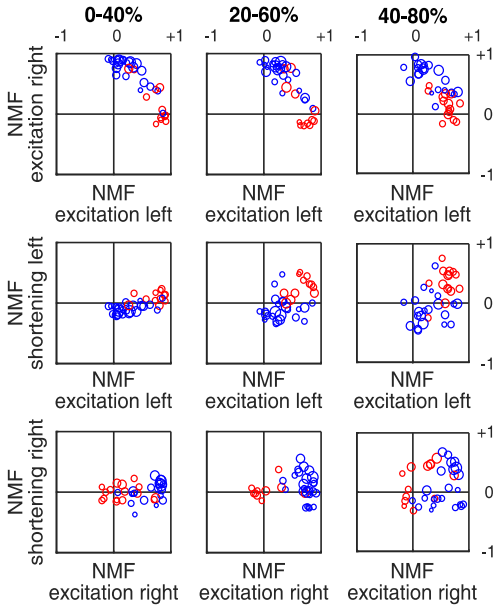

FIGURE 8. Correlation coefficients of NMF components (J = 6) and shortening and excitation profiles in the presence of significant muscle crosstalk. Results for excitation ranges 0-40%, 20-60% and 40-80% are depicted in different columns. Each circle represents a single NMF component, its relative size reflecting the energy accounted for in the preprocessed EMG signal. The components that contributed mostly to the lateral and the medial half of the EMG array in a single simulated muscle are depicted by blue and red circles, respectively.

were mostly correlated with either the medial or lateral group, many of them reflected both excitation profiles. The second and the third rows of Fig. 8 depict the impact of muscle shortening at different muscle excitation profiles. Unlike in the well separated cases of Fig. 5, the correlation values do not form tight clusters. In accordance with the well separated cases in Fig 5, the spread of the values increased with muscle excitation levels. This shows that, even in the presence of muscle crosstalk, there is a visible impact of muscle shortening on the muscle excitation estimations by NMF.

V. DISCUSSION

The results of this study demonstrate the ability of NMF to separate the contributions of different muscles when there is no significant crosstalk between different muscles in EMG recordings. Indeed, in the first experiment, we used two spatially well separated muscles, left and right BBs. As a result, there was no muscle crosstalk in the EMG signals, and the NMF separated the contributions of both muscles efficiently. Noteworthy, this is not the case in the presence of significant muscle crosstalk. We demonstrated this in the second experiment by simulating different excitation patterns of the medial and lateral heads of the BB, thus generating the EMG signals with large crosstalk. In this setup, many NMF components reflected contributions of both muscle heads. This agrees with our previous study on wrist flexors and extensors [17].

The impact of muscle shortening on muscle excitation estimation by NMF was relatively small at low excitation levels, but increased significantly with the excitation (Figs. 6 and 7 and Tables 1 and 2). At 0-20 % excitation and J = 2, the average correlation coefficient between the NMF components and the muscle shortening profiles was 0.08±0.01 (Table 2). At the same excitation range of 20 % but with minimum excitation value increased to 40 %, that is, with 40-60% excitation profile, these correlations increased to 0.41±0.026 (Table 2). Similar dependences of NMF components on muscle shortening profiles were observed in the presence of muscle crosstalk.

The sensitivity of NMF to muscle shortening also depended on the range of muscle excitation. Specifically, it decreased with the range (Figs. 6 and 7 and Tables 1 and 2), suggesting that the NMF components reflect the dynamics of muscle excitation, as well as the dynamics of muscle shortening in the EMG signals. In the case of relatively large excitation dynamics the impact of muscle shortening on NMF components was relatively limited (Figs. 6 and 7 and Tables 1 and 2). However, when excitation dynamics decreased, the relative impact of muscle shortening increased (Tables 1 and 2).

Increasing the number of NMF components J significantly increased the sensitivity of NMF to muscle shortening (Tables 1 and 2). For example, increasing J from 2 to 6 increased the correlation from 0.08 ± 0.01 to 0.19 ± 0.10 for 0-20 % excitation, and from 0.41 ± 0.026 to 0.62 ± 0.135 for 40-60 % excitation (Table 2). At the same time, the correlation between the NMF components and the excitation profiles decreased with J, from 0.95 ± 0.004 to 0.88 ± 0.056 for 0-20 % excitation, and from 0.82 ± 0.018 to 0.57 ± 0.136 for 40-60 % excitation (Table 1). The sensitivity to muscle shortening differed considerably for different identified components (Figs. 4 and 5), but without the known shortening and excitation profile, the component with the best excitation vs. shortening compromise is difficult to select. For this reason, we further analyzed the components that accounted for the largest percentage of EMG energy.

The correlation between the NMF component and muscle shortening depends on the extent of changes in the MUAP shapes (Fig. 1). In this study, the BB muscle was studied as one of the muscles with the largest geometrical changes in dynamic contractions. Furthermore, a relatively large range of muscle shortenings was studied (10-90 %). Therefore, the results of this study cannot be generalized easily to other skeletal muscles. For example, the results of decomposition of wrist flexors and extensors demonstrate relatively small MUAP changes during wrist movements [17]. Nevertheless, the MUAPs change with fatigue [16], [22] and in dynamic contractions in practically all the muscles, and further studies are required to quantify the sensitivity of NMF to MUAP changes in different experimental conditions.

Noteworthy, in this study, we selected the excitation and shortening profiles that were not correlated. This facilitated the analysis of NMF sensitivity to different profiles, and allowed for clear separation of excitation and shortening impacts. In healthy and unconstrained movements, the muscle excitation profile is likely to share several common characteristics with the shortening profile, though the extent of excitation and shortening similarities is yet to be evaluated carefully across many movement scenarios. Namely, in a constrained muscle, or in the presence of pathophysiology, such as during spasms or pathological co-activation after stroke, the excitation and shortening profiles of the investigated muscles can exhibit significantly different dynamics [30].

Finally, the muscle shortening is not the only source of MUAP changes. Significant and relatively fast MUAP changes are also caused by muscle fatigue, especially at higher excitation levels. Indeed, MUAP changes due to fatigue are comparable in size to the MUAP changes during dynamic contractions of the BB muscle (Fig. 1). Moreover, different MUs exhibit different levels of fatigue demonstration. Therefore, the NMF sensitivity to MUAP changes presented herein can very likely be extended to conditions with severe muscle fatigue.

ACKNOWLEDGMENT

The authors would like to thank Vojko Glaser and acknowledge his contributions in the preparation of the library of dynamic MUAPs, used in this study.

REFERENCES

[1] A. Holobar and D. Zazula, "Correlation-based decomposition of surface electromyograms at low contraction forces," *Med. Biol. Eng. Comput.*, vol. 42, no. 4, pp. 487–495, Jul. 2004, doi: 10.1007/BF02350989.
[2] A. Holobar and D. Zazula, "Multichannel blind source separation using convolution kernel compensation," *IEEE Trans. Signal Process.*, vol. 55, no. 9, pp. 4487–4496, Sep. 2007, doi: 10.1109/TSP.2007.896108.
[3] A. d'Avella, P. Saltiel, and E. Bizzi, "Combinations of muscle synergies in the construction of a natural motor behavior," *Nature Neurosci.*, vol. 6, no. 3, pp. 300–308, Feb. 2003, doi: 10.1038/nn1010.
[4] A. d'Avella, M. Giese, Y. P. Ivanenko, T. Schack, and T. Flash, "Editorial: Modularity in motor control: From muscle synergies to cognitive action representation," *Frontiers Comput. Neurosci.*, vol. 9, p. 126, Oct. 2015, doi: 10.3389/fncom.2015.00126.
[5] M. C. Tresch, V. C. K. Cheung, and A. d'Avella, "Matrix factorization algorithms for the identification of muscle synergies: Evaluation on simulated and experimental data sets," *J. Neurophysiol.*, vol. 95, no. 4, pp. 2199–2212, Apr. 2006, doi: 10.1152/jn.00222.2005.
[6] M. Chen, A. Holobar, X. Zhang, and P. Zhou, "Progressive FastICA peel-off and convolution kernel compensation demonstrate high agreement for high density surface EMG decomposition," *Neural Plasticity*, vol. 2016, pp. 1–5, Aug. 2016, doi: 10.1155/2016/3489540.
[7] S. A. Overduin, A. d'Avella, J. Roh, and E. Bizzi, "Modulation of muscle synergy recruitment in primate grasping," *J. Neurosci.*, vol. 28, no. 4, pp. 880–892, Jan. 2008, doi: 10.1523/JNEUROSCI.2869-07.2008.
[8] T. Lencioni, J. Jonsdottir, D. Cattaneo, A. Crippa, E. Gervasoni, M. Rovaris, E. Bizzi, and M. Ferrarin, "Are modular activations altered in lower limb muscles of persons with multiple sclerosis during walking? Evidence from muscle synergies and biomechanical analysis," *Frontiers Hum. Neurosci.*, vol. 10, p. 620, Dec. 2016, doi: 10.3389/fnhum.2016.00620.
[9] N. Hesam-Shariati, T. Trinh, A. G. Thompson-Butel, C. T. Shiner, and P. A. McNulty, "A longitudinal electromyography study of complex movements in poststroke therapy. 2: Changes in coordinated muscle activation," *Frontiers Neurol.*, vol. 8, p. 277, Jul. 2017, doi: 10.3389/fneur.2017.00277.
[10] M. Ghassemi, K. Triandafilou, A. Barry, M. E. Stoykov, E. Roth, F. A. Mussa-Ivaldi, D. G. Kamper, and R. Ranganathan, "Development of an EMG-controlled serious game for rehabilitation," *IEEE Trans. Neural Syst. Rehabil. Eng.*, vol. 27, no. 2, pp. 283–292, Feb. 2019, doi: 10.1109/TNSRE.2019.2894102.

[11] N. Wenger, E. M. Moraud, J. Gandar, P. Musienko, M. Capogrosso, L. Baud, C. G. L. Goff, Q. Barraud, N. Pavlova, N. Dominici, and I. R. Minev, "Spatiotemporal neuromodulation therapies engaging muscle synergies improve motor control after spinal cord injury," *Nature Med.*, vol. 22, no. 2, pp. 138–145, Feb. 2016, doi: 10.1038/nm.4025.
[12] D. Farina, I. Vujaklija, M. Sartori, T. Kapelner, F. Negro, N. Jiang, K. Bergmeister, A. Andalib, J. Principe, and O. C. Aszmann, "Man/machine interface based on the discharge timings of spinal motor neurons after targeted muscle reinnervation," *Nature Biomed. Eng.*, vol. 1, no. 2, pp. 1–12, Feb. 2017, doi: 10.1038/s41551-016-0025.
[13] M. Sartori, G. Durandau, S. Došen, and D. Farina, "Robust simultaneous myoelectric control of multiple degrees of freedom in wrist-hand prostheses by real-time neuromusculoskeletal modeling," *J. Neural Eng.*, vol. 15, no. 6, Oct. 2018, Art. no. 066026, doi: 10.1088/1741-2552/aae26b.
[14] F. Lunardini, C. Casellato, A. d'Avella, T. D. Sanger, and A. Pedrocchi, "Robustness and reliability of synergy-based myocontrol of a multiple degree of freedom robotic arm," *IEEE Trans. Neural Syst. Rehabil. Eng.*, vol. 24, no. 9, pp. 940–950, Sep. 2016, doi: 10.1109/TNSRE.2015.2483375.
[15] M. Sartori, D. G. Llyod, and D. Farina, "Neural data-driven musculoskeletal modeling for personalized neurorehabilitation technologies," *IEEE Trans. Biomed. Eng.*, vol. 63, no. 5, pp. 879–893, May 2016, doi: 10.1109/TBME.2016.2538296.
[16] R. M. Enoka, "Morphological features and activation patterns of motor units," *J. Clin. Neurophysiol.*, vol. 12, no. 6, pp. 538–559, Nov. 1995, doi: 10.1097/00004691-199511000-00002.
[17] M. Savc, V. Glaser, J. Kranjec, I. Cikajlo, Z. Matjacic, and A. Holobar, "Comparison of convolutive kernel compensation and non-negative matrix factorization of surface electromyograms," *IEEE Trans. Neural Syst. Rehabil. Eng.*, vol. 26, no. 10, pp. 1935–1944, Oct. 2018, doi: 10.1109/TNSRE.2018.2869426.
[18] A. Holobar, M. A. Minetto, and D. Farina, "Accurate identification of motor unit discharge patterns from high-density surface EMG and validation with a novel signal-based performance metric," *J. Neural Eng.*, vol. 11, no. 1, Jan. 2014, Art. no. 016008, doi: 10.1088/1741-2560/11/1/016008.
[19] A. Holobar, D. Farina, M. Gazzoni, R. Merletti, and D. Zazula, "Estimating motor unit discharge patterns from high-density surface electromyogram," *Clin. Neurophysiol.*, vol. 120, no. 3, pp. 551–562, Mar. 2009, doi: 10.1016/j.clinph.2008.10.160.
[20] D. Farina, A. Holobar, R. Merletti, and R. M. Enoka, "Decoding the neural drive to muscles from the surface electromyogram," *Clin. Neurophysiol.*, vol. 121, no. 10, pp. 1616–1623, Oct. 2010, doi: 10.1016/j.clinph.2009.10.040.
[21] S. H. Nawab, S.-S. Chang, and C. J. De Luca, "High-yield decomposition of surface EMG signals," *Clin. Neurophysiol.*, vol. 121, no. 10, pp. 1602–1615, 2010, doi: 10.1016/j.clinph.2009.11.092.
[22] R. Merletti, M. Aventaggiato, A. Botter, A. Holobar, H. Marateb, and T. M. M. Vieira, "Advances in surface EMG: Recent progress in detection and processing techniques," *Crit. Rev. Biomed. Eng.*, vol. 38, no. 4, pp. 305–345, 2010, doi: 10.1615/CritRevBiomedEng.v38.i4.10.
[23] M. Chen and P. Zhou, "A novel framework based on FastICA for high density surface EMG decomposition," *IEEE Trans. Neural Syst. Rehabil. Eng.*, vol. 24, no. 1, pp. 117–127, Jan. 2016, doi: 10.1109/TNSRE.2015.2412038.
[24] F. Negro, S. Muceli, A. M. Castronovo, A. Holobar, and D. Farina, "Multi-channel intramuscular and surface EMG decomposition by convolutive blind source separation," *J. Neural Eng.*, vol. 13, no. 2, Feb. 2016, Art. no. 026027, doi: 10.1088/1741-2560/13/2/026027.
[25] N. Jiang, K. B. Englehart, and P. A. Parker, "Extracting simultaneous and proportional neural control information for multiple-DOF prostheses from the surface electromyographic signal," *IEEE Trans. Biomed. Eng.*, vol. 56, no. 4, pp. 1070–1080, Apr. 2009, doi: 10.1109/TBME.2008.2007967.
[26] M. W. Berry, M. Browne, A. N. Langville, V. P. Pauca, and R. J. Plemmons, "Algorithms and applications for approximate nonnegative matrix factorization," *Comput. Statist. Data Anal.*, vol. 52, no. 1, pp. 155–173, Sep. 2007, doi: 10.1016/j.csda.2006.11.006.
[27] V. Glaser and A. Holobar, "Motor unit identification from high-density surface electromyograms in repeated dynamic muscle contractions," *IEEE Trans. Neural Syst. Rehabil. Eng.*, vol. 27, no. 1, pp. 66–75, Jan. 2019, doi: 10.1109/TNSRE.2018.2885283.
[28] A. J. Fuglevand, D. A. Winter, and A. E. Patla, "Models of recruitment and rate coding organization in motor-unit pools," *J. Neurophysiol.*, vol. 70, no. 6, pp. 2470–2488, Dec. 1993, doi: 10.1152/jn.1993.70.6.2470.
[29] E. Henneman, "Relation between size of neurons and their susceptibility to discharge," *Science*, vol. 126, no. 3287, pp. 1345–1347, Dec. 1957.
[30] B. Potocnik, M. Divjak, F. Urh, A. Francic, J. Kranjec, M. Savc, I. Cikajlo, Z. Matjacic, M. Zadravec, and A. Holobar, "Estimation of muscle co-activations in wrist rehabilitation after stroke is sensitive to motor unit distribution and action potential shapes," *IEEE Trans. Neural Syst. Rehabil. Eng.*, vol. 28, no. 5, pp. 1208–1215, May 2020, doi: 10.1109/TNSRE.2020.2980440.

MARTIN ŠAVC (Member, IEEE) received the B.Sc. and Ph.D. degrees in computer science from the Faculty of Electrical Engineering and Computer Science (FEECS), University of Maribor (UM), Slovenia, in 2011 and 2020, respectively. His research interests include signal processing, biomedical engineering, color image processing, machine learning, and computer vision applications.

ALEŠ HOLOBAR (Member, IEEE) received the Ph.D. degree in computer science from the Faculty of Electrical Engineering and Computer Science (FEECS), University of Maribor (UM), Slovenia. He is currently the Head of the System Software Laboratory, the Head of the Computer Science Institute, and a Full Professor with FEECS, UM. He has authored or coauthored more than 150 scientific articles published in peer-reviewed journals and conference proceedings. His main research interests include biomedical signal processing and biomedical imaging. He is a member of the ISEK, IAPR, Slovenian Society of Pattern Recognition, and Slovenian Society of Biomedical Engineering.